Int. J. Heat Mass Transfer. Vol. 33, No. 7, pp. 1441–1449, 1990
Printed in Great Britain

0017-9310/90 $3.00 + 0.00

Augmentation of natural convection heat transfer using binary gas coolants

J. G. PETRI and T. L. BERGMAN
Department of Mechanical Engineering, The University of Texas at Austin, Austin, TX 78712, U.S.A.

(*Received* 30 *June* 1989 *and in final form* 26 *September* 1989)

Abstract—An investigation has been conducted to ascertain the feasibility of augmenting natural convection heat transfer rates by using binary gas coolants. In this study, a helium-rich mixture which is seeded with a small amount of xenon yields higher heat transfer rates relative to those associated with pure helium. Experimental and analytical results imply that three mechanisms are in part and, to various degrees, responsible for the augmentation. Convective heat transfer rates are increased due to thermophysical property variation induced by seeding the helium with xenon. Prandtl effects limit augmentation while solutal buoyancy forces, which are established by thermal diffusion, are of minor importance.

INTRODUCTION

INTEREST has recently developed in natural convective heat transfer involving binary fluids. To date, applications such as materials processing have served as the motivation to study heat transfer in these fluids [1]. However, it has been suggested that binary mixtures can be used in other engineering applications, such as the passive cooling of electronic components, in order to enhance natural convective cooling rates [2]. The following discussion describes the potential advantages associated with the use of binary gas coolants in natural convection systems.

If a binary coolant is considered as a heat transfer fluid in a natural convection situation, heat transfer augmentation may occur due to an array of considerations. For example, augmentation may be due to the rather straightforward consequences of thermophysical property variation. For a specified geometry, the dimensionless natural convection heat transfer rate is related to the Rayleigh or Grashof number and the Prandtl number of the fluid. If variations in Pr are small, heat transfer correlations are typically of the form, $\overline{Nu} \propto Ra_T^n$. Using this proportionality, $\bar{h}$ for a particular geometry and applied temperature difference may be expressed as

$$\bar{h} \propto (c \cdot \rho^2/\mu)^n \cdot k^{1-n}. \quad (1)$$

Since n is positive but less than unity, it is apparent that $\bar{h}$ may be increased by selecting coolants characterized by large densities and thermal conductivities and, to a lesser extent, specific heats. High viscosity fluids are to be avoided.

In a similar fashion, pure coolants may be seeded with additives to tailor the thermophysical properties of the mixture. A specific coolant the thermal performance of which may be augmented in this manner is helium, which has the desirable feature of high thermal conductivity. A cursory inspection of the properties of noble gases suggests that mixtures of helium ($MW \cong 4$) and larger elements such as xenon ($MW \cong 131$) possess substantially increased ρ and, perhaps $\bar{h}$ may be increased. Indeed, Fig. 1 illustrates the degree of heat transfer augmentation which may be expected by adding X mole fraction of xenon to helium. Thermophysical properties are taken from the Appendix while Pr effects are assumed to be negligible. Augmentation, due merely to thermophysical property variation, is predicted to occur over narrow ranges of X and optimal blends exist because of the decreased thermal conductivity and increased viscosity of the mixtures relative to pure helium. The degree of augmentation increases with the exponent n.

The physical concepts used to develop Fig. 1 are straightforward and, of course, other blends may be identified. Upon further consideration of binary coolants, however, it becomes evident that other phenomena may serve to augment heat transfer rates as well. Because of the disparate molecular weights of helium and xenon, for example, significant solutal buoyancy forces may be established by cross-diffusion. Despite the general disregard of these processes in heat transfer applications, their influence on the natural convection of binary fluids can be significant [3, 4].

Species gradients are established by Soret diffusion if a binary fluid is subjected to a temperature gradient. Returning to the helium–xenon system as an example, heavy xenon is diffused toward cold temperature regions. As a result, thermal and solutal buoyancy forces will presumably act in unison to drive natural convection. To quantify solutal buoyancy forces, a dimensionless stability parameter may be evaluated to estimate the relative magnitude of Soret-induced solutal to thermal buoyancy forces within the system [3]

$$\gamma = k_T \cdot \beta_C / \bar{T} \cdot \beta_T \quad (2)$$

NOMENCLATURE

c	specific heat
C	xenon mass fraction
D	binary diffusion coefficient
g	gravitational acceleration
k	thermal conductivity
k_T	thermal diffusion coefficient
$\bar{h}$	average heat transfer coefficient
Le	Lewis number, Sc/Pr
MW	molecular weight
n	exponent on Ra
$\overline{Nu}$	average Nusselt number
P	pressure
q'	heat rate per unit length
r	radius
R	inside radius of the pressure vessel
Ra_T	thermal Rayleigh number
S	separation parameter
Sc	Schmidt number
T	temperature
u	θ component of the velocity
v	r component of the velocity
X	mole fraction of xenon.

Greek symbols

β	expansion coefficient
γ	dimensionless stability ratio
δ	heated plate height
θ	angular coordinate, dimensionless temperature
μ	dynamic viscosity
ρ	mass density.

Subscripts

c	solutal, cold
h	hot
ref	reference
T	thermal
0	pure helium.

Superscript

$\bar{}$	average.

where $\bar{T}$ is the average temperature of the mixture. The stability parameter varies with X as shown in the Appendix and it is noted that the maximum γ value is 0.55 at $X = 0.08$. Tantalizingly, Soret-induced solutal gradients may increase density variations within the coolant by 50%, leading to even greater heat transfer augmentation than implied in Fig. 1. Other effects attributable to Soret diffusion, such as the diffusion of high thermal conductivity, helium-rich fluid toward heated surfaces, may serve to decrease the heat transfer resistance of the coolant even further.

Based on the previous discussion, it is evident that a binary coolant, such as helium–xenon, may offer a decreased convective heat transfer resistance relative to pure helium. Furthermore, the degree of augmentation cannot be determined beforehand, since solutal buoyancy forces may significantly impact convective transport mechanisms. As such, the objective of this study is to investigate natural convective heat transfer using, as an example, the binary helium–xenon system. As will become evident, this strategy elucidates the role of solutal buoyancy forces for the particular geometry considered here.

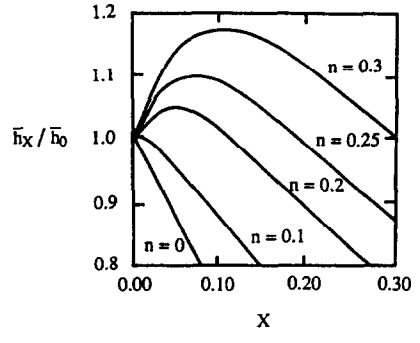

FIG. 1. Potential natural convective heat transfer enhancement resulting from seeding helium with a xenon additive.

THE EXPERIMENTS

A series of experiments was performed in order to measure heat transfer augmentation associated with binary gas coolants. The helium–xenon system was selected due to the availability of reliable thermophysical property information and due to the disparate molecular weights of the constituents. A total of 15 experiments, using three different power inputs, were conducted using various helium–xenon mixtures.

The experiments were performed in a test cell consisting of a heated vertical isothermal plate held within a sealed cylindrical pressure vessel as shown in Fig. 2. A positive coolant pressure of two atmospheres was imposed to prohibit air leakage into the enclosure.

The heated plate consists of a 0.005 mm thick resistive heating element sandwiched between two polished 0.8 mm thick, 25.4 × 356 mm copper sheets. Four 0.1 mm diameter copper–constantan thermocouples were installed in fine grooves machined in the inner surfaces of the copper plates and placed 12.7 mm from the bottom edge of the vertical plate at axial locations of 22, 100, 192 and 289 mm. The plate was situated in the center of the cylindrical pressure vessel which was equipped with appropriate hardware to allow for vessel evacuation, gas pressurization and measurement of the quantities of interest.

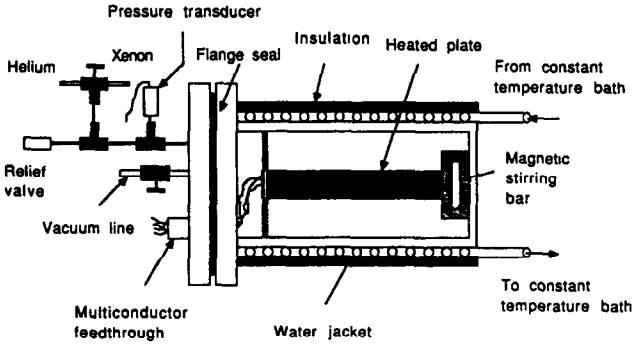

FIG. 2. Schematic of the test cell and instrument connections.

The pressure vessel was constructed of a 102 mm nominal diameter stainless steel pipe with a 9.5 mm wall thickness. The pipe is capped at one end and a 136 kg (300 lb) stainless steel neck is butt-welded to the opposite end. A 136 kg (300 lb) stainless steel blind, which houses all of the gas and instrumentation connections, is mounted to the neck and sealed with high vacuum grease providing for negligible helium leakage during an individual experiment. A multiconductor feedthrough is threaded into the blind and houses electrically-insulated copper and constantan feedthrough studs which are used as the electrical connections to the thermocouples and the resistance heater.

The inner polished wall of the pressure vessel serves as the cold surface in the experiments. It is kept at a constant temperature by a water jacket formed of tubing wrapped around the outer surface of the vessel. Temperature differences across the vessel wall are negligible. The tubing and vessel are insulated from the laboratory and three thermocouples are mounted on the interior wall of the vessel in order to measure its temperature. The coolant pressure is measured by a semiconductor strain gage transducer which is used to determine the partial pressures of the gas components during vessel filling and to detect potential leakage during the course of an experiment.

The vessel is evacuated and held under high vacuum conditions for approximately 6 h prior to the start of each experiment. After introducing research grade helium and xenon into the vessel in the desired proportions, the gases are mixed for approximately 10 h by placing the vessel vertically on a heated magnetic stirrer. The stirring rod is positioned inside a cage at the capped end of the vessel. After mixing, the vessel is leveled on a horizontal rack and heating and data acquisition commences. Typically, 3–4 h is sufficient time to ensure that steady state conditions have been achieved. The temperature of the vertical plate is determined by averaging the readout of the two thermocouples closest to the plates' center, since slight end cooling effects exist. In addition, the thermocouple output is averaged over the final 5 min of the experiment because small fluctuations ($\pm 0.02^{\circ}$C) occur during steady state operation due to instrument noise. The temperature measurements were corrected to account for radiative transfer and all of the instrumentation was calibrated prior to each experiment [5]. The uncertainty in the temperature measurements is $\pm 0.05^{\circ}$C and the uncertainty in X, for a particular experiment, is ± 0.006, as determined by the sequential perturbation method [6].

THE MODEL

Since optical access to the system is restricted and the xenon concentration variations within the coolant are small and immeasurable, it is prudent to develop analytical methodologies to predict local system behavior in order to identify the physical mechanisms responsible for heat transfer augmentation.

The computational system is shown in Fig. 3. A two-dimensional domain is considered and consists of an infinitely-thin heated plate of height δ, held concentrically within a cooled cylindrical enclosure of radius R. Since the system is symmetric about the vertical center line, only half of the enclosure is modeled.

Natural convection occurs in the binary coolant and the species separate by Soret effects which, in turn, establish solutal buoyancy forces in the system. The governing equations which describe the thermal response of the system are conservation of mass, momentum, energy and species. Coupling between the conserved quantities occurs due to thermosolutal

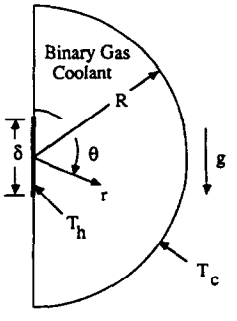

FIG. 3. Schematic of the coordinate system.

buoyancy contributions in the momentum equations and Soret diffusion of the xenon. The thermophysical properties of the fluid are assumed to be constant at any X, the Boussinesq approximation is invoked and the flow is taken to be laminar, steady and two-dimensional. The Dufour effect is of second order importance and is neglected. Although radiative transfer occurs between the plate and the cold vessel wall and can be significant, it is ignored in order to focus attention on the natural convection phenomena in the binary gas mixture.

The governing equations are:

continuity

$$\frac{1}{r}\frac{\partial}{\partial r}(\rho r v)+\frac{1}{r}\frac{\partial}{\partial \theta}(\rho u)=0; \quad (3)$$

θ momentum

$$\frac{1}{r}\frac{\partial}{\partial r}(\rho r u v)+\frac{1}{r}\frac{\partial}{\partial \theta}(\rho u u)$$
$$=\frac{1}{r}\frac{\partial}{\partial r}\left(\mu r\frac{\partial u}{\partial r}\right)+\frac{1}{r}\frac{\partial}{\partial \theta}\left(\frac{\mu \partial u}{r\partial \theta}\right)-\frac{1}{r}\frac{\partial P}{\partial \theta}$$
$$+2\frac{\mu}{r^2}\frac{\partial v}{\partial \theta}-\frac{\mu u}{r^2}-\frac{\rho u v}{r}-[g\beta_T\rho(T-T_{ref})$$
$$-g\beta_C\rho(C-C_{ref})]\cdot[\cos(\pi/2-\theta)]; \quad (4)$$

r momentum

$$\frac{1}{r}\frac{\partial}{\partial r}(\rho r v v)+\frac{1}{r}\frac{\partial}{\partial \theta}(\rho u v)$$
$$=\frac{1}{r}\frac{\partial}{\partial r}\left(\mu r\frac{\partial v}{\partial r}\right)+\frac{1}{r}\frac{\partial}{\partial \theta}\left(\frac{\mu \partial v}{r\partial \theta}\right)-\frac{\partial P}{\partial r}$$
$$-\frac{\mu v}{r^2}-\frac{2\mu}{r^2}\frac{\partial u}{\partial \theta}+\frac{\rho u^2}{r}+[g\beta_T\rho(T-T_{ref})$$
$$-g\beta_C\rho(C-C_{ref})]\cdot[\sin(\pi/2-\theta)]; \quad (5)$$

energy

$$\frac{1}{r}\frac{\partial}{\partial r}(\rho r v T)+\frac{1}{r}\frac{\partial}{\partial \theta}(\rho u T)$$
$$=\frac{1}{r}\frac{\partial}{\partial r}\left(\frac{kr\partial T}{c\partial r}\right)+\frac{1}{r}\frac{\partial}{\partial \theta}\left(\frac{k\partial T}{rc\partial \theta}\right); \quad (6)$$

species

$$\frac{1}{r}\frac{\partial}{\partial r}(\rho r v C)+\frac{1}{r}\frac{\partial}{\partial \theta}(\rho u C)=\frac{1}{r}\frac{\partial}{\partial r}\left(\rho D r\cdot\frac{\partial C}{\partial r}\right)$$
$$+\frac{1}{r}\frac{\partial}{\partial \theta}\left(\frac{\rho D}{r}\cdot\frac{\partial C}{\partial \theta}\right)+\frac{1}{r}\frac{\partial}{\partial r}\left(rDk_T/\bar{T}\cdot\frac{\partial T}{\partial r}\right)$$
$$+\frac{1}{r}\frac{\partial T}{\partial \theta}\left(\frac{\rho D}{r}k_T/\bar{T}\cdot\frac{\partial T}{\partial \theta}\right). \quad (7)$$

The last two terms on the RHS of equation (7) describe Soret diffusion of xenon [7].

The boundary conditions are associated with no-slip, impermeable walls with a specified temperature on the plate and the cold wall.

$$u=0 \quad \text{at} \quad r=R \quad \text{and at} \quad 0\leqslant r\leqslant R, \theta=0,\pi \quad (8)$$

$$v=0 \quad \text{at} \quad r=R \quad \text{and at} \quad 0\leqslant r\leqslant \delta.2, \theta=0,\pi \quad (9)$$

$$\partial v/\partial\theta=0 \quad \text{at} \quad \delta/2\leqslant r\leqslant R, \theta=0,\pi \quad (10)$$

$$\partial C/\partial r=-k_T/\bar{T}\cdot\partial T/\partial r \quad \text{at} \quad r=R \quad (11)$$

$$\partial C/\partial\theta=-k_T/\bar{T}\cdot\partial T/\partial\theta \quad \text{at} \quad \theta=0,\pi \quad (12)$$

$$T=T_h \quad \text{at} \quad 0\leqslant r\leqslant \delta/2, \theta=0,\pi \quad (13)$$

$$T=T_c \quad \text{at} \quad r=R \quad (14)$$

$$\partial T/\partial\theta=0 \quad \text{at} \quad \delta/2\leqslant r\leqslant R, \theta=0,\pi. \quad (15)$$

Normalization of the governing equations yields the following dimensionless parameters which govern system response:

thermal Rayleigh number

$$Ra_T=g\beta_T\delta^3\Delta T/\nu\cdot\alpha \quad (16)$$

Prandtl number $Pr=\nu/\alpha$ (17)

Schmidt number $Sc=\nu/D$ (18)

dimensionless plate size $\delta^*=\delta/R$ (19)

separation parameter $S=(k_T/\bar{T})\cdot\Delta T$ (20)

and the stability parameter of equation (2). The parameters in equations (16), (17) and (19) apply to natural convection involving a pure fluid in the geometry of interest while the Schmidt number is the ratio of momentum to species diffusivities and the separation parameter is a measure of the potential species concentration differences within the system.

The governing equations were discretized using the control volume approach while the power law formulation was used to determine the combined advective and diffusive fluxes across the control surfaces. The line-by-line procedure was used to solve the matrix equations and the SIMPLER algorithm was used to determine the pressure distribution within the system [8]. Additional terms in the momentum equations and the Soret diffusion terms of the species equation were treated as sources in the numerical procedure. An integral constraint was placed on the species concentration in order to enforce global species conservation, as described in ref. [2].

A uniform, 30×30 numerical grid provides fine spatial resolution adjacent to the heated plate and was used in all of the simulations. Model predictions were validated by comparing them with the experimental results.

RESULTS

Experimental results and numerical predictions indicate that natural convection heat transfer is aug-

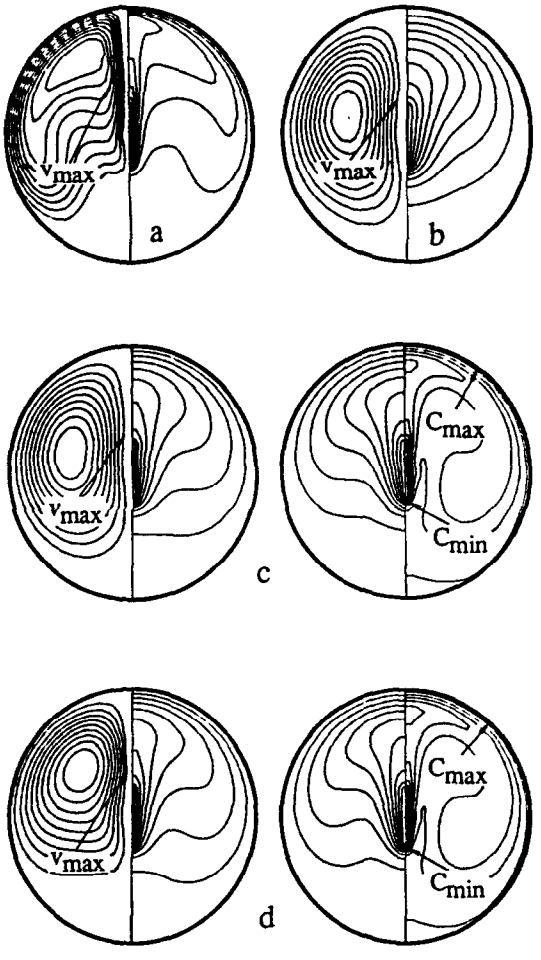

FIG. 4. Predicted streamlines, density isograms, isotherms and xenon concentration isopleths for $q' = 2.34$ W m^{-1}. (a) Air, $v_{max} = 45.7$ mm s^{-1}. (b) $X = 0.00$, $v_{max} = 19.5$ mm s^{-1}. (c) $X = 0.05$, $v_{max} = 30.3$ mm s^{-1}, $C_{max} = 0.6334$, $C_{min} = 0.6325$. (d) $X = 0.10$, $v_{max} = 35.0$ mm s^{-1}, $C_{max} = 0.7849$, $C_{min} = 0.7842$. All contours are shown in even increments between the maximum and minimum values.

mented by using the gas additive concept. As will become evident, varying degrees of augmentation occur due to a variety of physical phenomena.

Predicted and measured augmentation of natural convective heat transfer

Figure 4 includes numerical predictions which illustrate the augmentation of natural convection cooling with the use of binary gaseous coolants. Here, the plate temperature was adjusted numerically until a heat rate of approximately 2.34 W m^{-1} was predicted. Results are shown for air (Fig. 4(a)), pure helium (Fig. 4(b)) and two different helium–xenon mixtures (Figs. 4(c) and (d)). Predicted streamlines and isotherms are shown for the air and helium cases while predicted density isograms and xenon concentration isopleths are included for the binary coolant results. Locations and values of the maximum (and minimum) vertical velocities (xenon concentrations) are included in the figure.

A comparison of Figs. 4(a) and (b) illustrates the benefits which occur as the pure coolant is changed. When air is used, the gas density and buoyancy forces are large, resulting in substantial convective mixing and correspondingly large temperature gradients near the heated component, relative to the mixing and gradients for pure helium. However, due to the high thermal conductivity of helium, the plate temperature is significantly less ($\Delta T = 3.52$°C) than that associated with air ($\Delta T = 7.11$°C).

The simulations of Figs. 4(c) and (d) are associated with binary mixtures of $X = 0.05$ and 0.10, respectively. As X increases, the increased coolant density results in enhanced mixing relative to the pure helium results and induces steeper temperature gradients adjacent to the heated component. The warm plate is cooled more effectively and T_h is 3.23 and 3.28 K warmer than T_c for $X = 0.05$ and 0.10, respectively. As suggested by these results, optimum X values exist to minimize the operating temperature of the plate.

Xenon distributions within the coolant are quite complicated. In general, large concentration gradients coexist with large temperature gradients. Xenon gradients are, however, more severe than their thermal counterparts, since $Le = Sc/Pr > 1$. The maximum xenon concentration exists in the vicinity of the maximum thermal gradients at the cold wall (near the edge of the thermal plume which rises from the plate) and a film of xenon-rich fluid slides to the bottom of the enclosure. The lower portion of the enclosure is relatively stagnant with nearly uniform temperature, xenon concentration and density distributions.

Experimental results suggest that augmentation occurs when the binary fluid is used, as implied by the dimensionless heat transfer results of Fig. 5. The data are slightly below a correlation for heat transfer from a vertical plate in a quiescent environment (with $Pr = 0.7$) [9] because of the slight warming of the average fluid temperature within the enclosure. Since the scatter in the data is potentially due to Pr and/or γ influences which are, at this point unknown, the results are correlated without taking these effects into account and are best described by

$$\overline{Nu} = 0.565 Ra_T^{0.237}. \quad (21)$$

In corroboration with the predictions of Fig. 4, the contents and results of Fig. 1 and equation (21) suggest that an 8% increase in $\bar{h}$ will occur at $X = 0.075$, if Prandtl and Soret effects are not important.

Measured and predicted q' values are included in Table 1 for all of the experimental conditions. Excellent agreement is evident with the average and maximum difference between the experimental and numerical results being 1.5 and 5%, respectively. Hence, the numerical model is considered to be verified and can be used to determine the relative importance of solutal buoyancy in determining system performance.

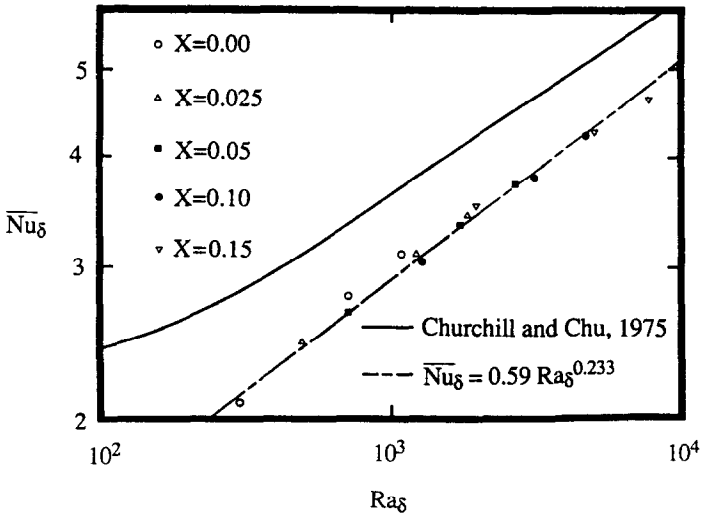

FIG. 5. Experimental heat transfer results for the various coolants.

Variations in heat transfer augmentation

To quantify the heat transfer augmentation offered by the binary mixture, a dimensionless plate temperature is defined as

$$\theta \equiv \Delta T/\Delta T_0 \tag{22}$$

which is, of course, inversely related to $\bar{h}$. Figure 6 shows the measured and predicted thermal performance resulting from use of binary fluid mixtures for various values of X and q'.

As discussed previously, if Pr and γ influences are not significant and $\overline{Nu} \propto Ra_T^n$, identical levels of augmentation must occur at a given X, regardless of q'. Since different degrees of augmentation are evident in Fig. 6 for the different power rates, Prandtl and/or Soret effects must be significant and are also responsible for the slight scatter of the dimensionless heat transfer data of Fig. 5. Although it is well known that increases in Pr generally increase natural convective heat transfer rates, reconsideration of the significant γ values for the helium–xenon pair does not allow one to dismiss the potential importance of solutal buoyancy forces. It is not possible to quantify either Soret or Prandtl influences using the experimental data. As such, the model is used to identify the cause of the unexpected results of Fig. 6.

Figures 7 and 8 include predictions associated with Experiments G and H. In these simulations, the operating temperature of the vertical plate is identical to the measured temperature listed in Table 1. The predictions include only thermal buoyancy forces (Figs. 7(a) and 8(a)), only solutal buoyancy forces (Figs. 7(b) and 8(b)) and thermosolutal buoyancy forces (Figs. 7(c) and 8(c)). Since the actual species separation is predicted, a modified stability ratio, $\gamma^* = \beta_C \cdot \Delta C/\beta_T \cdot \Delta T$, may be used to quantify solutal buoyancy effects.

Figures 7 and 8, which are typical of simulations

Table 1. Comparison of measured and predicted heat transfer rates for all of the experiments

Experiment	X	ΔT(°C)	q'_{exp} (W m^{-1})	q'_{num} (W m^{-1})	Percentage difference (%)
A	0.00	3.52	2.32	2.342	0.95
B	0.00	8.25	7.11	6.999	1.56
C	0.00	12.39	11.95	11.688	2.19
D	0.025	3.24	2.34	2.320	0.85
E	0.025	7.93	7.15	7.157	0.10
F	0.025	11.98	12.00	11.910	0.75
G	0.050	3.23	2.34	2 375	1.50
H	0.050	7.87	7 15	7.218	0.95
I	0.050	11.93	12.00	12.030	0.25
J	0.100	3.28	2.33	2.408	3.35
K	0.100	8.00	7.14	7.268	1.79
L	0.100	12.11	11.98	12.054	0.58
M	0.150	3.38	2.33	2 448	5.06
N	0.150	8.22	7.12	7.192	1.01
O	0.150	12.60	11.93	12.090	1.34

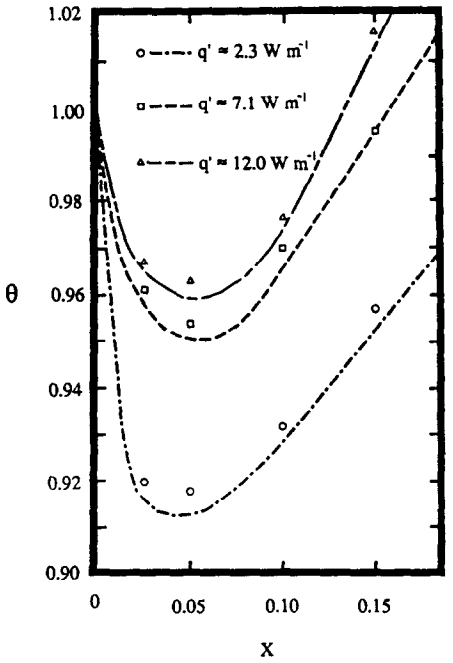

FIG. 6. Measured and predicted heated plate temperatures normalized by the $X = 0.00$ results.

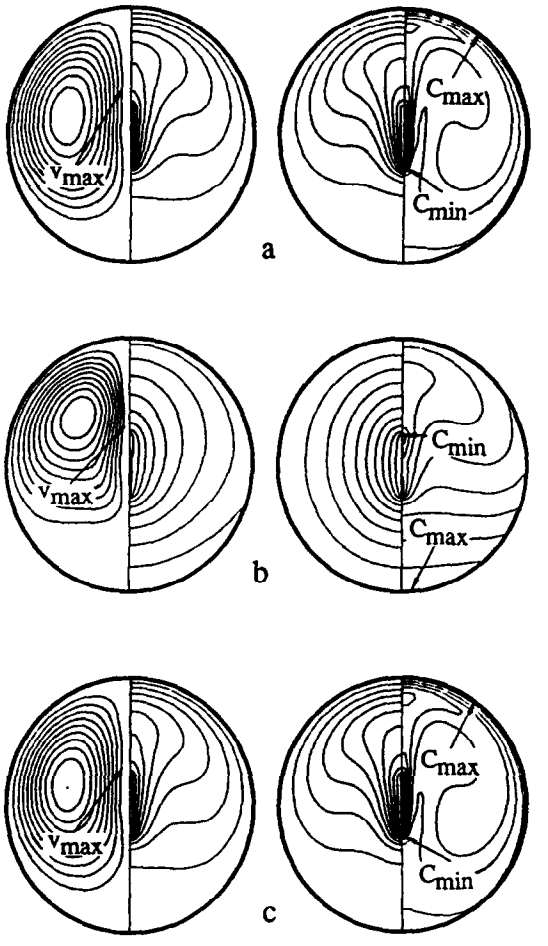

FIG. 7. Predicted streamlines, density isograms, isotherms and xenon concentration isopleths for $X = 0.05$ and $\Delta T = 3.23$°C. The predictions are associated with (a) thermal buoyancy forces only, $v_{max} = 30.3$ mm s^{-1}, $C_{max} = 0.6334$, $C_{min} = 0.6325$, (b) solutal buoyancy forces only, $v_{max} = 5.1$ mm s^{-1}, $C_{max} = 0.6340$, $C_{min} = 0.6322$ and (c) thermosolutal buoyancy forces, $v_{max} = 30.3$ mm s^{-1}, $C_{max} = 0.6334$ and $C_{min} = 0.6325$. All contours are shown in even increments between the maximum and minimum values.

with β_C or $\beta_T = 0$ for other X and q', share common features. Specifically, comparisons of Figs. 7(a) and (c), as well as Figs. 8(a) and (c) indicate that the convective characteristics of the system are nearly unchanged as solutal buoyancy is accounted for. Maximum vertical velocities are only slightly modified and the predicted species separations are nearly identical, regardless of whether or not β_C is included in the simulations. Xenon separation is decreased by convective mixing, relative to the degree of separation implied by γ (≈ 0.50) and γ^* values are 0.208 and 0.218 in Figs. 7(c) and 8(c), respectively.

Figures 7(b) and 8(b) reveal that solutal buoyancy forces are present and sufficient to drive residual convection within the system. Solutally driven convection is, however, weak relative to the thermally driven flow and, due to the decreased mixing in the system, the xenon separation increases relative to the case where β_T is accounted for. Xenon-laden gas fills the bottom of the enclosure and helium-rich fluid lines the warm plate. Pockets of low xenon concentration fluid exist near the top and bottom of the heated plate, as expected from consideration of the conduction solution [5].

The relevant heat transfer result of Figs. 7 and 8 is the variation of the predicted heat transfer rate as solutal buoyancy forces are included in the analysis. In the low power case (Fig. 7) the plate heat transfer rate is increased only marginally from 2.371 to 2.376 W m^{-1} as Soret-induced buoyancy forces are included in the analysis. For the high power case (Fig. 8) the heat transfer rate is decreased from 7.232 to 7.218 W m^{-1} as β_C is accounted for. Hence, Soret diffusion has a slight effect on the heat transfer in the system, but not to the degree implied by the value of γ. Moreover, solutal buoyancy forces can decrease convective heat transfer rates. Since $Le \neq 1$ solutal and thermal buoyancy forces do not coexist spatially and are not necessarily additive effects. The results of Figs. 7 and 8, as well as simulations for other experimental conditions, show that solutal buoyancy effects tend to spread the curves of Fig. 6, but are not of sufficient strength to affect the augmentation mechanism to a significant degree. As such, the variation in the heat transfer augmentation at any X is due to other effects.

In general, $\overline{Nu}_\delta$ increases with Pr in natural convection systems and, with the exception of the lowest Ra_T, $X = 0.00$ result (and to a lesser extent the results for $X = 0.15$, $Ra_T \approx 2000$) this trend is observed in Fig. 5. Hence, for the intermediate and high q' cases,

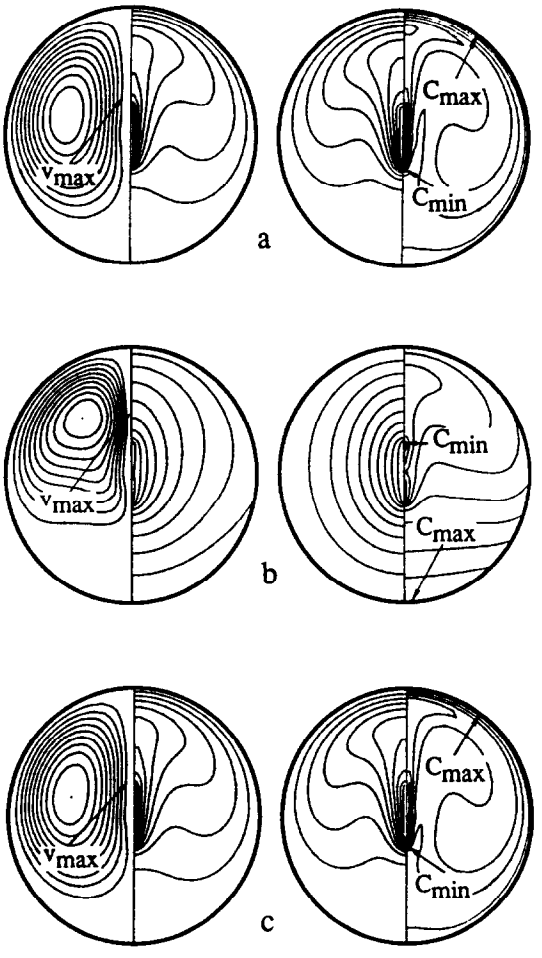

FIG. 8. Predicted streamlines, density isograms, isotherms and xenon concentration isopleths for $X = 0.05$ and $\Delta T = 7.87$°C. The predictions are associated with (a) thermal buoyancy forces only, $v_{max} = 50.2$ mm s^{-1}, $C_{max} = 0.6338$, $C_{min} = 0.6315$, (b) solutal buoyancy forces only, $v_{max} = 8.1$ mm s^{-1}, $C_{max} = 0.6349$, $C_{min} = 0.6311$ and (c) thermosolutal buoyancy forces, $v_{max} = 49.4$ mm s^{-1}, $C_{max} = 0.6338$ and $C_{min} = 0.6315$. All contours are shown in even increments between the maximum and minimum values.

Pr effects limit augmentation to levels below those suggested by Fig. 1. The more significant enhancement for the low q' case is due to changes in the convective flow structure at extremely low Ra_δ. A series of numerical simulations revealed that, for $300 \leqslant Ra_o \leqslant 1000$, the bottom of the enclosure transforms from a thermally active state (Fig. 4(b)) to a thermally inactive condition as Ra_δ is increased and the amount of inactivity increases with Ra_o [5]. As such, the value of n decreases with increasing Ra_o and augmentation of the helium system at low Ra_δ is greater than suggested by equation (21).

SUMMARY AND CONCLUSIONS

The motivation for this study was to identify alternative methods for passively enhancing the natural convection cooling of heated components. Preliminary considerations suggested that enhancement may be achieved by seeding pure coolants with high molecular weight additives. For the helium–xenon system, enhancement was speculated to occur by a combination of thermophysical property variation and the development of solutal buoyancy forces induced by Soret diffusion.

The measured and predicted levels of cooling enhancement resulting from xenon seeding are in excellent agreement. With validation of the numerical model, it was determined that variations in the level of enhancement occur as the xenon mole fraction and applied power level are varied. For the system considered here, the enhancement is due, almost solely, to thermophysical property variation and solutal buoyancy forces are not of sufficient strength to affect the system's behavior. In fact, solutal buoyancy can decrease heat transfer rates slightly, since the temperature and species distributions do not coincide spatially.

The results and conclusions of this study are limited to the geometry considered here and care must be taken in applying the results to other cooling situations. Specifically, variations in the convective flow structure and the fashion in which the Soret-induced species distribution develops within the enclosure will be different for other geometries and heating conditions. Hence, variations in the amount of heat transfer augmentation and the importance of solutal buoyancy forces are problem dependent [2].

Acknowledgements—The authors gratefully acknowledge various sources of support for this research. We would like to thank the National Science Foundation for sponsorship under Grant No. CBT-8552806 and acknowledge the use of computational facilities provided by the Department of Mechanical Engineering at The University of Texas at Austin. The experiments were made possible by a University of Texas at Austin Endowed Faculty Fellowship and the kind assistance of Professor Gary Vliet and Mr Francisco Cosenza.

REFERENCES

1. R. Viskanta, T. L. Bergman and F. P. Incropera, Double-diffusive natural convection. In *Natural Convection: Fundamentals and Applications* (Edited by S. Kakaç *et al.*), pp. 1075–1099. Hemisphere, Washington, DC (1985).
2. T. L. Bergman and J. G. Petri, Natural convection cooling of discrete heated elements in an enclosure using pressurized helium–xenon gas mixtures. In *Natural and Mixed Convection in Electronic Equipment Cooling* (Edited by R. A. Wirtz), pp. 25–33. American Society of Mechanical Engineers, New York (1988).
3. J. K. Platten and J. C. Legros, *Convection in Liquids*. Springer, Berlin (1985).
4. J. R. Abernathey and F. Rosenberger, Soret diffusion and convective stability in a closed vertical cylinder. *Physics Fluids* **24**, 377–381 (1981).
5. J. G. Petri, Augmentation of natural convection cooling

Table 2. Selected thermophysical properties of the helium–xenon mixture at $\bar{T} = 350$ K and $P = 2$ atm

X	$\rho(\mathrm{kg\,m^{-3}})$	$k(\mathrm{W\,m^{-1}K^{-1}})$	$c(\mathrm{J\,kg^{-1}K^{-1}})$	$\mu(\mathrm{N\,s\,m^{-1}})$	$D(\mathrm{m^2\,s^{-1}})$	k_T	β_C	Pr	Sc	γ
0.00	1.116	0.156	5192.6	19.5×10^{-6}	—	—	—	0.649	—	—
0.05	2.890	0.136	2004.4	22.8	8.36×10^{-6}	0.208	2.511	0.336	0.943	0.522
0.08	3.955	0.125	1464.8	23.9	8.48	0.160	3.435	0.280	0.713	0.550
0.10	4.663	0.118	1242.4	24.4	8.55	0.134	4.052	0.257	0.612	0.544
0.15	6.439	0.102	899.8	24.9	8.45	0.089	5.594	0.220	0.458	0.501
0.20	8.211	0.087	705.6	25.0	8.35	0.062	7.135	0.203	0.365	0.447

using binary gas mixtures, M.S. Thesis, The University of Texas at Austin, Austin, Texas (1989).
6. R. J. Moffat, Describing the uncertainties in experimental results, *Exp. Therm. Fluid Sci.* **1**, 3–17 (1988).
7. D. Gutkowicz-Krusin, M. A. Collins and J. Ross, Rayleigh Benard instability in nonreactive binary fluids. I: theory, *Physics Fluids* **22**, 1443–1450 (1979).
8. S. V. Patankar, *Numerical Heat Transfer and Fluid Flow*. Hemisphere, Washington, DC (1980).
9. S. W. Churchill and H. H. S. Chu, Correlating equations for laminar and turbulent free convection from a vertical plate, *Int. J. Heat Mass Transfer* **18**, 1323–1327 (1975).
10. Y. S. Touloukian and C. Y. Ho, *Thermophysical Properties of Matter*. Plenum Press, New York (1972).
11. J. O. Hirschfelder, C. F. Curtiss and R. B. Bird, *Molecular Theory of Gases and Liquids*. Wiley, New York (1954).

APPENDIX

Thermophysical properties of the helium–xenon gas mixture are shown in Table 2 for selected xenon mole fractions. The properties were determined as follows.

The average molecular weight of the mixture is

$$\overline{MW} = X\cdot MW_{\text{xenon}} + (1-X)\cdot MW_{\text{helium}} \tag{A1}$$

while the mass fraction of component i is

$$C_i = X_i\cdot MW_i/\overline{MW}. \tag{A2}$$

The gas density and specific heats may be determined by approximating the mixture as an ideal gas while the thermal conductivity and absolute viscosity are taken from ref. [10]. The Lewis number of the mixture is reported in ref. [4], from which D may be evaluated. The values of k_T and β_C are determined by the methods outlined in ref. [11].

AUGMENTATION DE LA CONVECTION THERMIQUE NATURELLE PAR UTILISATION DE REFRIGERANTS GAZEUX BINAIRES

Résumé—On étudie la possibilité d'accroître le transfert thermique par convection naturelle en utilisant des gaz réfrigérants binaires. Un mélange riche en hélium avec une faible proportion de xenon conduit à des flux thermiques plus grands que pour l'hélium pur. Les résultats expérimentaux et analytiques impliquent trois mécanismes qui interviennent, à des degrés différents, dans cet accroissement. Les flux thermiques convectés sont augmentés à cause de la variation de propriétés physiques résultant du mélange de l'hélium avec le xenon. L'effet du nombre de Prandtl limite l'augmentation tandis que les forces de flottement solutales qui s'établissent par diffusion thermique sont de moindre importance.

ERHÖHUNG DER WÄRMEABFUHR DURCH NATÜRLICHE KONVEKTION BEI VERWENDUNG EINES BINÄREN GASGEMISCHES

Zusammenfassung—Es wurde eine Untersuchung durchgeführt, um die Möglichkeit einer Verbesserung der Kühlung durch natürliche Konvektion bei Verwendung eines binären Gasgemisches zu bestätigen. In dieser Arbeit wird Helium mit einer geringen Menge Xenon geimpft, was zu einer Verbesserung des Wärmeübergangs gegenüber der Verwendung von reinem Helium führt. Die experimentellen und analytischen Ergebnisse deuten auf drei Mechanismen hin, die—in unterschiedlichem Ausmaß—für die Verbesserung verantwortlich sind. Der konvektive Wärmeübergang wird durch eine Veränderung der thermophysikalischen Eigenschaften infolge der Impfung mit Xenon verbessert. Einflüsse der Prandtl-Zahl begrenzen die Verbesserung, während konzentrationsbedingte Auftriebskräft von geringerer Wichtigkeit sind.

ИНТЕНСИФИКАЦИЯ ЕСТЕСТВЕННОКОНВЕКТИВНОГО ТЕПЛОПЕРЕНОСА ПРИ ИСПОЛЬЗОВАНИИ В КАЧЕСТВЕ ХЛАДАГЕНТОВ БИНАРНЫХ ГАЗОВЫХ СМЕСЕЙ

Аннотация—Проведено исследование с целью определения возможности интенсификации естественноконвективного теплопереноса за счет использования в качестве хладагентов бинарных газовых смесей. При введении небольшого количества ксенона в гелий приводит к возрастанию интенсивности теплопереноса. Полученные экспериментальные и аналитические результаты позволяют сделать вывод о том, что эта интенсифкация обусловлена в различной степени действием трех механизмов. Измененне теплофизических свойств, связанное с введением ксенона в гелий, вызывает возрастание интенсивности конвективного теплопереноса. Прандтлевские эффекты ограничивают интенсификацию, тогда как действующие на примесь архимедовы силы, порождаемые тепловой диффузией, играют незначительную роль.